RSC Advances

PAPER

View Article Online
View Journal | View Issue

Cite this: *RSC Adv.*, 2020, **10**, 5864

Synthesis, intermolecular interactions and biological activities of two new organic–inorganic hybrids $C_6H_{10}N_2$,2Br and $C_6H_{10}N_2$,2Cl·H_2O†

Intissar Hamdi,[a] Intidhar Bkhairia,[*b] Andreas Roodt,[c] Thierry Roisnel,[d] Moncef Nasri[b] and Houcine Naïli[*a]

Received 8th November 2019
Accepted 10th January 2020

DOI: 10.1039/c9ra09294c

rsc.li/rsc-advances

A slow evaporation method has permitted the crystallization of two novel crystals of (2-aminomethyl) pyridindiumdihalide $C_6H_{10}N_2$,2Br (**1**) and $C_6H_{10}N_2$,2Cl·H_2O (**2**). The structures of the prepared compounds (**1**) and (**2**) were elucidated by single-crystal X-ray diffraction which revealed that they crystallize, respectively, with triclinic and monoclinic symmetries. Their crystal packing was stabilized by non-covalent interactions, including N–H···Br, C–H···Br, N–H···Cl, O–H···Cl and N–H···O hydrogen bonds. 3-D Hirshfeld surface analysis followed by 2-D fingerprint schemes gives insights into the intermolecular interactions in the crystalline structure. Furthermore, the FT-IR spectroscopy of these two compounds was carried out. The synthesized products were also screened for *in vitro* antioxidant and antimicrobial activities, which reveals their favourable antioxidant activities against 1,1-diphenyl-2-picrylhydrazyl (DPPH) as well as the discolouration of β-carotene.

1. Introduction

In the last twenty years, studies on the self-assembly of molecular salts as well as their hydrogen-bond interactions in the solid-state have evoked a multitude of interest among chemists owing to their intriguing structural diversities and potential applications.[1] Weak intermolecular interactions which are important in the fields of physical, chemical and life sciences represent the backbone of self-assembly processes and supramolecular architectures and exert directional and saturation effects.[2–5] The hydrogen bond, which is the most common among weak interactions, remains the most important and reliable means of enforcing molecular organization in the solid-state,[6–13] plays a critical role in many chemical and biological processes, and has been a subject of research interest.[14–16] To enrich the varieties in such kinds of hybrid compounds and to investigate the influence of hydrogen bonds on the structural features, we aimed to use the amine 2-(aminomethyl)pyridine (amp) also commonly known as 2-picolylamine (pic) a clear yellowish liquid used as an intermediate in the pharmaceutical industry[17–21] for obtaining two new amine halide salts $C_6H_{10}N_2$,2Br and $C_6H_{10}N_2$,2Cl·H_2O which are expected to possess notable chemical and biological activities.

2. Experimental

2.1. Materials

All the employed chemicals, hydrochloric acid (HCl; 37%), hydrobromic acid (HBr; 48%) and 2-aminomethyl pyridine (2-picolylamine ($C_6H_8N_2$); 99%) were commercial products (Sigma-Aldrich), which were used without further purification.

2.2. Synthesis

Compounds (**1**) and (**2**) were prepared by mixing 2-picolylamine (1 mmol; 0.108 g) and 10 mL of distilled water. The resulting solutions were acidified with concentrated hydrobromic acid (1 mmol; 5 drops) for (**1**) and hydrochloric acid (1 mmol; 5 drops) for (**2**). The two mixture were stirred magnetically for 10 min at room temperature resulting in the formation of homogeneous solutions. The two resulting solutions were slowly evaporated to dryness for a week. Some single crystals with suitable dimensions for crystallographic study were collected. The synthesis is reproducible and crystals prepared in this way are stable for a long time under normal conditions of temperature and humidity.

[a]*Laboratory of Physico-chemical of the Solid State, Department of Chemistry, Faculty of Sciences of Sfax, Université de Sfax, BP 1171, 3000 Sfax, Tunisia. E-mail: houcine_naili@yahoo.com; Fax: +216 74 274 437; Tel: +216 98 660 026*

[b]*Laboratory of Enzyme Engineering and Microbiology, University of Sfax, National School of Engineering of Sfax (ENIS), B.P. 1173-3038 Sfax, Tunisia. E-mail: ibkhairia@yahoo.com*

[c]*Department of Chemistry, University of the Free State, P.O. Box 339, Bloemfontein 9300, South Africa*

[d]*University of Rennes, CNRS, ISCR (Institute of Chemical Sciences of Rennes) – UMR 6226, F-35000 Rennes, France*

† Electronic supplementary information (ESI) available. CCDC 1919004 and 1919003 contain the supplementary crystallographic data for (**1**) and (**2**), respectively. For ESI and crystallographic data in CIF or other electronic format see DOI: 10.1039/c9ra09294c

2.3. Infrared spectroscopy

IR absorption spectra of the title compounds were measured with a PerkinElmer BX FT-IR spectrometer, in the 400–4000 cm^{-1} region at ambient temperature with KBr pellets.

2.4. Single-crystal X-ray data collection and structure determination

Crystal data, data collection and structure refinement details for (**1**) and (**2**) are summarized in Table 1. Data for crystals (**1**), were collected on a Bruker D8 VENTURE AXS diffractometer using Mo-Kα radiation. The structure was solved by the dual-space algorithm using the SHELXT program[22] and then refined with full-matrix least-squares methods based on F^2(SHELXL).[23] All non-hydrogen atoms were refined with anisotropic atomic displacement parameters. Except nitrogen linked hydrogen atoms that were introduced in the structural model through Fourier difference maps analysis, H atoms were finally included in their calculated positions. A final refinement on F^2 with 2065 unique intensities and 104 parameters converged at $\omega R(F^2) = 0.046$ ($R(F) = 0.019$) for 1928 observed reflections with $I > 2\sigma(I)$. The reflection data for (**2**) was collected on APEX II area detector 4-circles diffractometer using graphite monochromated Mo-Kα radiation ($\lambda = 0.71073$ Å), with ω- and φ-scans at 100(2) K, through the Bruker AXS APEX2 software. The crystal structure was solved in the monoclinic symmetry, space group $P2_1/c$ and according to the automated search for space group available in WingX,[24] which incorporates SHELXL.[25] In the structure refinement, all hydrogen atoms were added in calculated positions and treated as riding on the atom to which they are attached. All non-hydrogen atoms were refined with anisotropic displacement parameters. The hydrogen atoms were positioned geometrically and refined, utilizing a riding model fixed C–H distance of 0.93 Å (CH) for aromatic hydrogen, and methylene H-atoms fixed at 0.97 Å (CH). Bond distances and angles calculated from the final atomic coordinates, as well as probable hydrogen bonds, are listed in Tables 2 and 3. The drawings were made with Diamond program.[26]

2.5. Hirshfeld surface analyses

The intermolecular interactions ensuring the structure cohesion are visualized by Hirshfeld surface analysis and the 2-D fingerprint plots which identify each type of intermolecular interactions. The Hirshfeld surfaces and 2-D fingerprint plots were prepared in this paper by means of Crystal Explorer (Version 3.1)[27] based on the structure of the CIF file. The Hirshfeld surface is set using (d_{norm}). The measured connection distance (d_{norm}) is determined on the basis of d_e and d_i by,

Table 1 Crystallographic data for $C_6H_{10}N_2$,2Br and $C_6H_{10}N_2$,2Cl·H_2O

Empirical formula	$C_6H_{10}N_2$,2Br	$C_6H_{10}N_2$,2Cl·H_2O
Formula weight (g mol^{-1})	269.98	199.08
Temperature (K)	150	293
Wavelength (Å)	0.71073	0.71073
Crystal system	Triclinic	Monoclinic
Space group	$P\bar{1}$	$P2_1/c$
a (Å)	6.6560 (9)	16.678 (5)
b (Å)	7.7563 (10)	7.107 (5)
c (Å)	9.1524 (12)	15.865 (5)
α (°)	76.320 (4)	90
β (°)	80.652 (4)	97.397 (5)
γ (°)	82.187 (5)	90
V ($Å^3$)	450.65 (10)	1864.8 (15)
Z	2	8
Calculated density (mg m^{-3})	1.990	1.418
Absorption coefficient (mm^{-1})	8.93	0.65
F(000)	260	832
Crystal size (mm^3)	0.33 × 0.27 × 0.16	0.33 × 0.27 × 0.16
Habit-color	Plate-colourless	Block-yellow
$\theta_{min} - \theta_{max}$ (°)	3.1–27.5	1.2–28.4
R_{int}	0.041	0.041
T_{min}	0.103	0.811
T_{max}	0.240	0.902
Index ranges	$-8 \le h \le 8$	$-22 \le h \le 20$
	$-10 \le k \le 10$	$-9 \le k \le 7$
	$-11 \le l \le 11$	$-21 \le l \le 20$
Refinement method	Full-matrix least-squares on F^2	Full-matrix least-squares on F^2
R_1	0.020	0.025
wR_2	0.046	0.092
Goodness-of-fit on F^2	1.05	1.19
Data/restraints/parameters	2065/0/104	4666/0/215
Extinction coefficient	0.075 (3)	0.066 (5)
$\Delta\rho_{min}$ (e $Å^{-3}$)	−0.75	−0.40
$\Delta\rho_{max}$ (e $Å^{-3}$)	0.65	0.39

Table 2 Selected bond distances (Å) and angles (°) for (1) and (2)

$C_6H_{10}N_2$,2Br			
N1–C5	1.343 (3)	C2–C3	1.383 (3)
N1–C1	1.344 (3)	C5–C4	1.384 (3)
N2–C6	1.492 (3)	C5–C6	1.505 (3)
C2–C1	1.376 (3)	C4–C3	1.387 (3)
C5–N1–C1	123.64 (17)	C5–C4–C3	119.14 (19)
C1–C2–C3	119.14 (19)	C2–C3–C4	120.29 (19)
N1–C5–C4	118.67 (17)	N1–C1–C2	119.11 (19)
N1–C5–C6	116.61 (17)	N2–C6–C5	111.10 (16)
C4–C5–C6	124.71 (18)		
$C_6H_{10}N_2$,2Cl·H_2O			
N3–C7	1.3431 (17)	C2–C4	1.3805 (18)
N3–C1	1.3471 (16)	C2–C10	1.5054 (17)
N4–C11	1.3431 (17)	C3–C5	1.3914 (18)
N4–C2	1.3483 (16)	C4–C9	1.3967 (18)
N5–C10	1.4745 (17)	C4–C9	1.3967 (18)
N6–C12	1.4777 (18)	C6–C11	1.376 (2)
C1–C3	1.3856 (18)	C6–C9	1.3898 (19)
C1–C12	1.5089 (17)	C7–C8	1.3780 (19)
C7–N3–C1	123.10 (11)	C2–C4–C9	119.67 (12)
C11–N4–C2	123.18 (11)	C3–C5–C8	119.86 (12)
N3–C1–C3	118.64 (11)	C11–C6–C9	118.46 (12)
N3–C1–C12	116.49 (11)	N3–C7–C8	120.09 (12)
C3–C1–C12	124.82 (12)	C7–C8–C5	118.64 (12)
N4–C2–C4	118.49 (11)	C6–C9–C4	119.97 (12)
N4–C2–C10	115.00 (11)	N5–C10–C2	112.67 (11)
C4–C2–C10	126.46 (12)	N4–C11–C6	120.22 (12)
C1–C3–C5	119.65 (12)	N6–C12–C1	111.65 (11)

$$d_{norm} = \frac{d_i - r_i^{vdW}}{r_i^{vdW}} + \frac{d_e - r_e^{vdW}}{r_e^{vdW}}$$

where r_i^{vdW} and r_e^{vdW} are the van der Waals radii of the atoms. d_i and d_e are the distance from Hirshfeld surface to nearest nucleus inside and to nearest nucleus outside, respectively. The d_{norm} value can be negative or positive. The d_{norm} values are set using a red-white-blue color scheme.[28,29] The short contact is red, the white indicates the contact around vdW, and the blue is for longer contact. Fingerprint areas represent a combination of bi-directional $d_e - d_i$ and $d_i - d_e$ measures. The graph shows that the areas visible in the fingerprint correspond to a single molecule, such as $d_e > d_i$ and the other $d_i > d_e$. The 2-D fingerprint segment provides quantitative analysis of the molecular interconnections found in the molecule and presents this information in a plot of color.[30]

2.6. Antioxidant and antibacterial activities

2.6.1. Antioxidant activities

2.6.1.1. ABTS radical scavenging activity. According to the method of Wang *et al.*[31] ABTS radical scavenging activity of $C_6H_{10}N_2$,2Br and $C_6H_{10}N_2$,2Cl·H_2O was determined. This method is based on the ability of the compounds to trap the $ABTS^{+\bullet}$ radical cation. 1 mL of test compounds, at different concentrations (0.5 to 2 mg mL^{-1} dissolved in dimethylsulphoxide (DMSO)), were as mixed with 1 mL the preformed radical (ABTS) and then kept in obscurity at room temperature, the residual absorbance of the $ABTS^{+\bullet}$ radical is measured at 734 nm. In the presence of antioxidant compounds (**1** and **2**), the nitrogen radical concerned scavenge an $H^{\bullet}$, leading to $ABTSH^{+}$, which causes the formation of a precipitate and discoloration of the solution.

The ABTS scavenging activity was calculated by the following formula:

$$\text{ABTS scavenging activity}(\%) = \frac{A_{control} - A_{sample}}{A_{control}} \times 100 \quad (1)$$

where $A_{control}$ is the absorbance control and A_{sample} is the absorbance of $C_6H_{10}N_2$,2Br and $C_6H_{10}N_2$,2Cl·H_2O sample.

2.6.1.2. β-Carotene-linoleic-acid assay. The ability of $C_6H_{10}N_2$,2Br (**1**) and $C_6H_{10}N_2$,2Cl·H_2O (**2**) to prevent bleaching of β-carotene was assessed as described by Koleva *et al.*[32] A stock solution of β-carotene/linoleic acid mixture was freshly prepared before each experiment. 2.5 mL of the emulsion of β-carotene/linoleic acid were transferred to test tubes containing two crystals concentrations. The tubes were immediately placed in water bath and incubated at 50 °C for 2 h. The absorbance of each hybrid compound was measured at 470 nm. The same

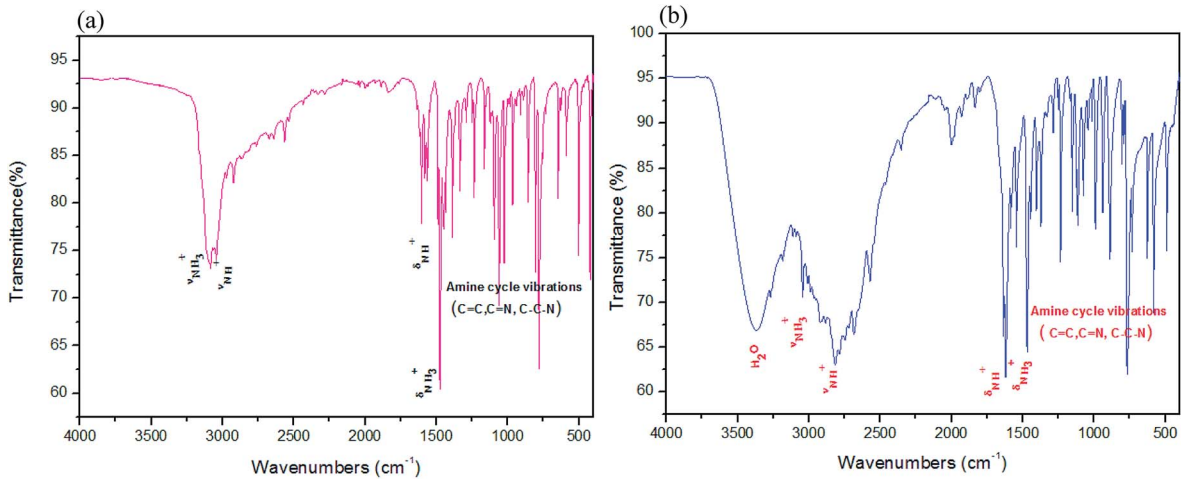

Fig. 1 IR spectra of $C_6H_{10}N_2$,2Br (a), and $C_6H_{10}N_2$,2Cl·H_2O (b).

procedure was repeated with butylated hydroxyanisole (BHA) as positive control. A blank consisted of 0.5 mL of distilled water instead of sample. Antioxidant activity in β-carotene bleaching model in percentage was calculated with the following equation:

$$\beta\text{-Carotene-bleaching inhibition}(\%) = \left[1 - \frac{(A_0 - A_t)}{\left(A_0' - A_t'\right)}\right] \times 100 \quad (2)$$

where A_0 and A_0' are the absorbance of the sample and the control, respectively, measured at time zero, and A_t and A_t' are the absorbance of the sample and the control, respectively, measured after 2 h.

2.6.1.3. Ferric ion reducing antioxidant power (FRAP). The reducing power was performed according to the method of Xie *et al.*[33] 1 mL of each crystal sample at different concentrations (0.5–2 mg mL^{-1}) was mixed with 1.25 mL of phosphate buffer (pH = 6.6; 0.2 M) and 2.5 mL of potassium ferricyanide (1% (w/v)) solution. The reaction tubes were incubated for 20 min at 50 °C. After incubation, 2.5 mL of trichloroacetic acid (TCA, 10% (w/v)) was added and the reactions mixtures were then centrifuged for 10 min at 10 000 × *g*. 2.5 mL of supernatant, from each hybrid compound mixture, was mixed with distilled water (2.5 mL) and ferric chloride (0.5 mL of 0.1% (w/v)) solution. The absorbance of the resulting solutions was measured at 700 nm.

2.6.1.4. DPPH assay. The DPPH radical-scavenging activity of the two crystals was determined according to the method of Bersuder *et al.*[34] Briefly, 0.5 mL of each hybrid compound at different concentrations (0.5–2 mg mL^{-1}) was added to 0.375 mL of ethanol and 0.125 mL of a DPPH solution prepared in ethanol (0.02% (w/v)). The reaction solutions were incubated in the dark at room temperature for 60 min. Scavenging capacity was measured spectrophotometrically at 517 nm. DPPH radical-scavenging activity was calculated as follows:

$$\text{DPPH radical scavenging activity}(\%) = \frac{A_{\text{control}} + A_{\text{blank}} - A_{\text{sample}}}{A_{\text{control}}} \quad (3)$$

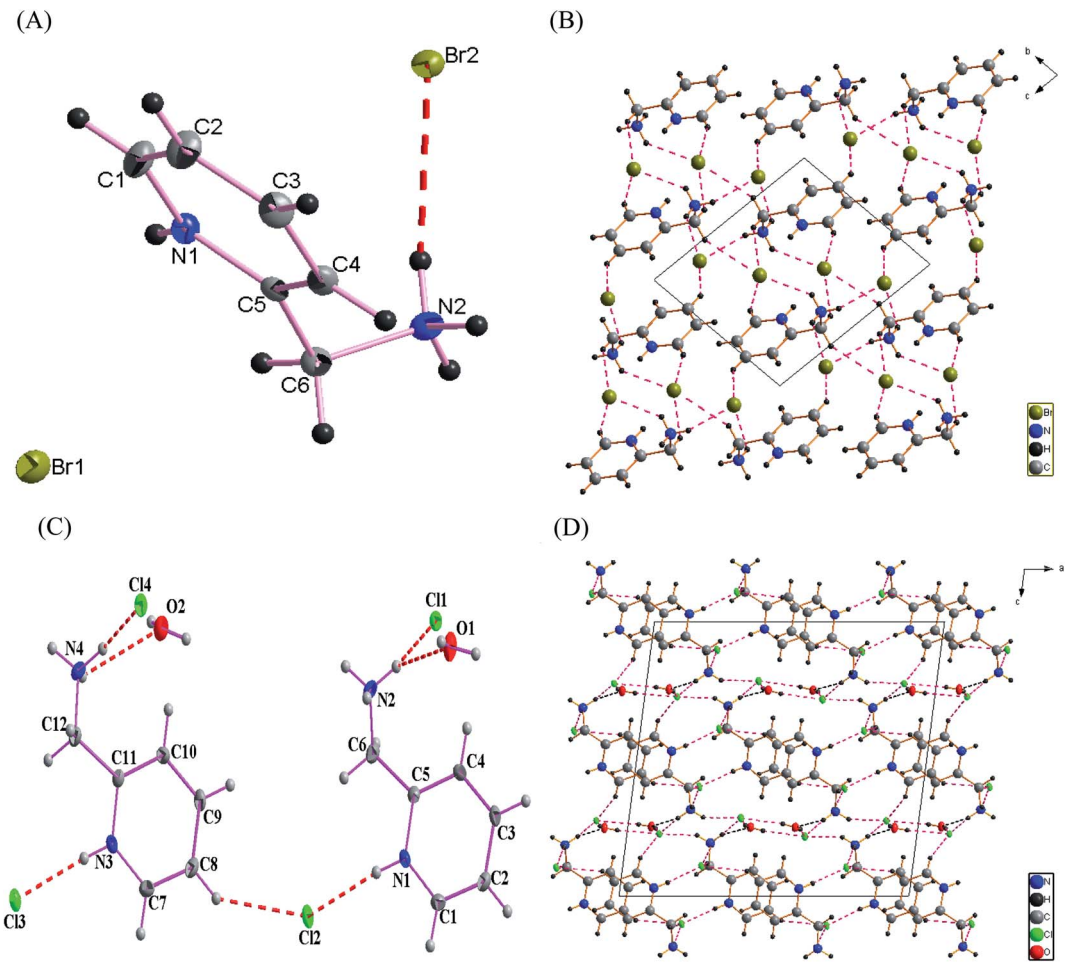

Fig. 2 (A) The asymmetric unit of compound (**1**), showing the atom-labeling scheme. Displacement ellipsoids are drawn at 50% probability level. The dashed line represents the possible hydrogen bond. (B) The crystal packing of the title salt (**1**) projected onto *bc* plane. The N–H···Br and C–H···Br hydrogen bonds are shown as dashed lines. (C) The asymmetric unit of compound (**2**), showing the atom-labeling scheme. Displacement ellipsoids are drawn at 50% probability level. The dashed lines represent the possible hydrogen bonds. (D) A view of the three-dimensional supramolecular architecture of (**2**), formed by N–H···Cl, O–H···Cl and N–H···O hydrogen bond interactions.

where $A_{control}$ is the absorbance of the control reaction, A_{blank} is the absorbance of the blank and A_{sample} is the absorbance of the sample with DPPH solution. BHA was used as a positive control.

2.6.2. Antibacterial activities

2.6.2.1. Microorganisms. Antibacterial activities of the synthesized compounds were tested against Gram$^+$ and Gram$^-$ bacterial strains. Bacteria used were *Bacillus cereus* (ATCC 11778), *Staphylococcus aureus* (ATCC 25923), *Enterococcus faecalis* (ATCC 29212), *Salmonella enterica* (ATCC 43972), *Micrococcus luteus* (ATCC 4698), and *Klebsiella pneumoniae* (ATCC 13883).

2.6.2.2. Agar-well diffusion method. The antibacterial potential was essayed by agar-well diffusion method as described by Tagg and McGiven.[35] 200 μL of freshly cell suspension adjusted to 10^6 cfu mL^{-1} for bacteria were speared onto the surface of agar. After incubation, wells (6 mm in diameter) were punched in the agar medium with sterile Pasteur pipettes and 50 μL of the hybrid compound (20 mg mL^{-1}) was added to each well. Gentamicin and bacitracin (150 μg mL^{-1}) was used as positive control to determine the sensitivity of each bacterial strain. To permit the diffusion of the hybrid compound and standards onto agar, the plate was allowed to stand for 4 h at 4 °C. After that, the plate was incubated at 37 °C for 24 h. The antimicrobial activity was evaluated by determination of the inhibition zone diameters (IZD).

3. Results and discussion

3.1. Infrared spectroscopy

In both IR spectra (Fig. 1a and b for **1** and **2**, respectively), the presence of the 2-aminomethyl pyridindium was checked, indeed the bands appearing around 1500 and 3110 cm^{-1} on each IR spectrum are assigned, respectively, to the deformation and elongation vibrations of the NH_3^+ group. In addition, the

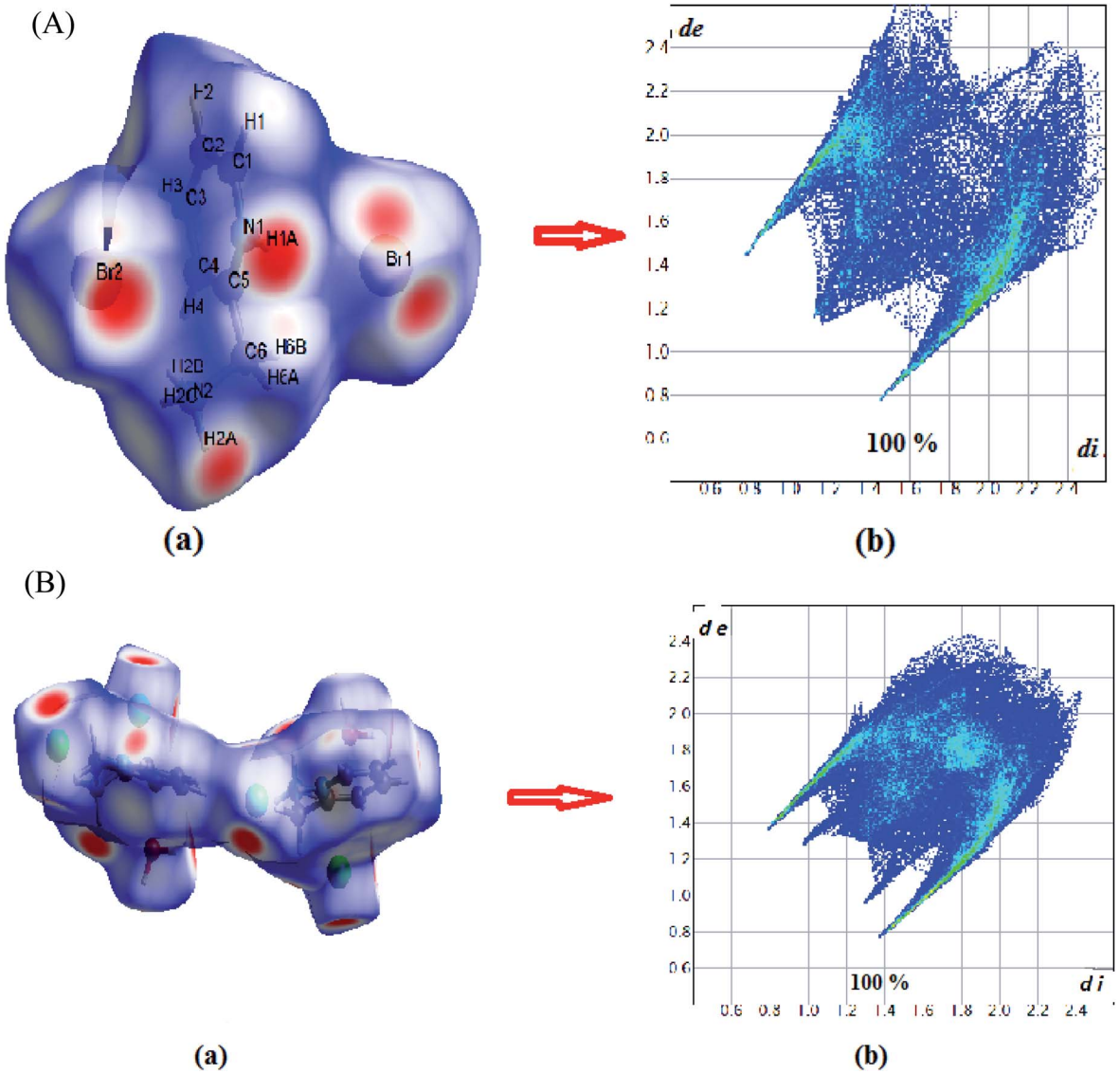

Fig. 3 (A) Hirshfeld surface mapped over d_{norm} (a) of the asymmetric unit and 2D fingerprint plots (b) of the $C_6H_{10}N_2$,2Br compound. (B) Hirshfeld surface mapped over d_{norm} (a) of the asymmetric unit and 2D fingerprint plots (b) of the $C_6H_{10}N_2$,2Cl·H_2O compound.

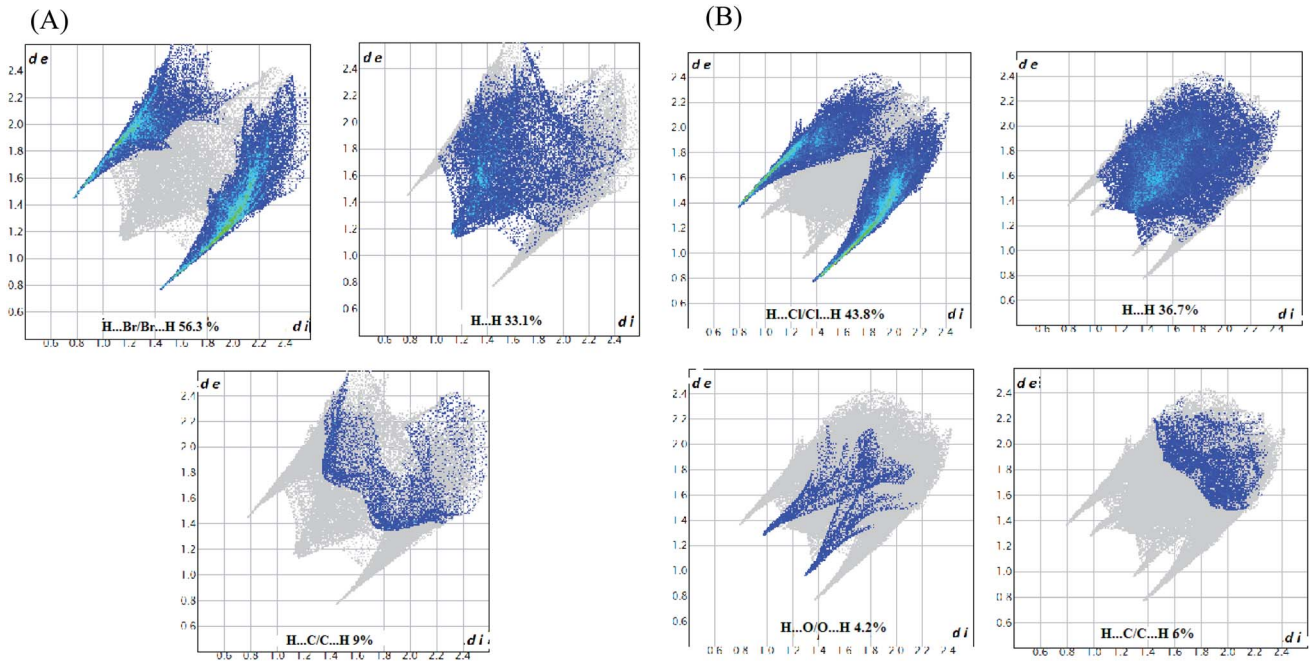

Fig. 4 (A) 2D fingerprint plots of the $C_6H_{10}N_2$,2Br compound. (B) 2D fingerprint plots of the $C_6H_{10}N_2$,2Cl·H_2O compound.

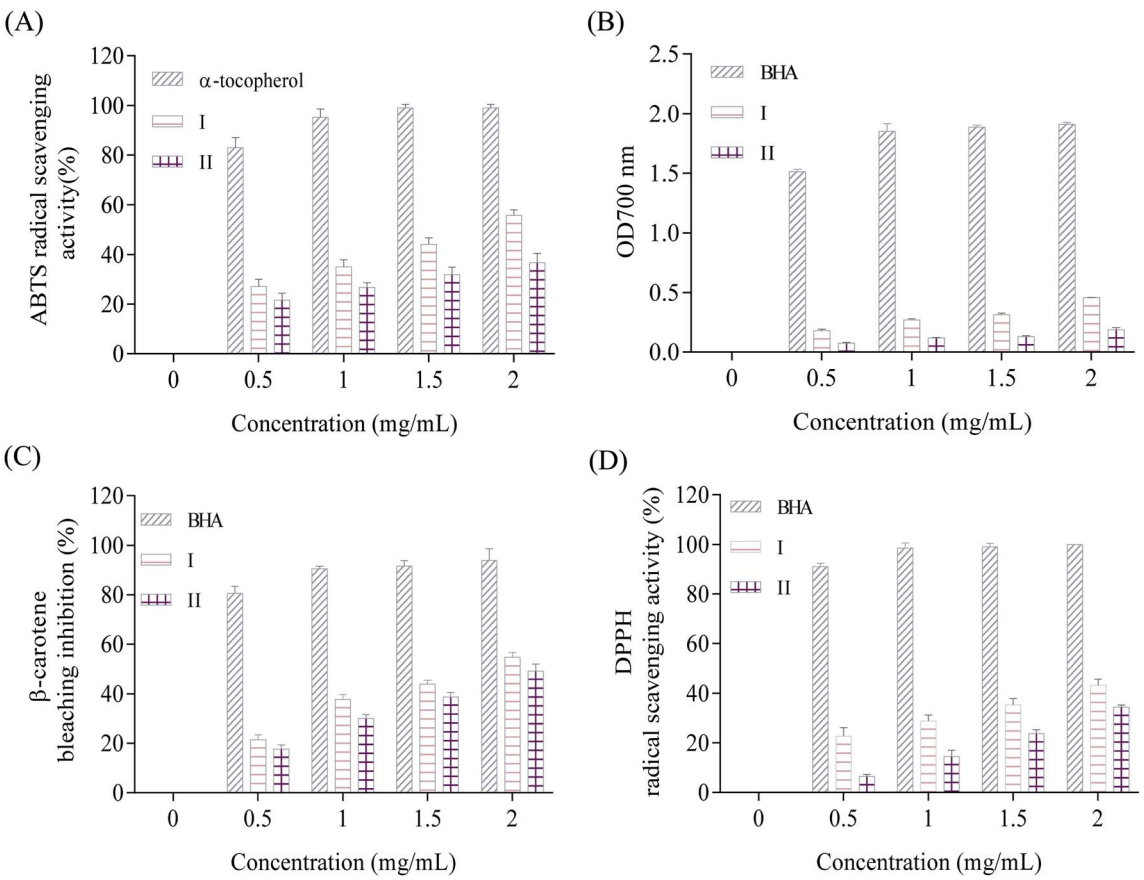

Fig. 5 (A) ABTS radical scavenging of compounds (1) and (2) at different concentration. (B) Reducing power of the synthesized compounds (1) and (2) at different concentrations. C) β-Carotene bleaching inhibition activity of the synthesized compounds (1) and (2) at different concentrations. (D) DPPH free radical-scavenging activity of compounds (1) and (2) at different concentrations.

bands around 1635 and 3071 cm^{-1} can be assigned, respectively, to the NH^+ deformation and elongation vibrations which corroborate the protonation of the 2-picolylamine molecule. The bands with different intensities between 500 and 1400 cm^{-1} are due to the vibrations of the amine cycle. The IR spectrum of compound (**2**) shows a large band around 3353 cm^{-1} which can be attributed to the vibrations of the water molecule.

3.2. Structural commentary

The structure of (**1**) is solved in the triclinic space group $P\bar{1}$ (Table 1) with an asymmetric unit consisting of two bromide anions and one diprotonated 2-aminomethyl pyridine cation, which are connected together *via* N–H···Br and C–H···Br hydrogen bonds as shown in Fig. 2(A). Selected bond lengths, angles, and supramolecular interactions are listed in Tables 2 and 3, respectively. The cohesion is ensured by hydrogen bonds between the cationic groups and the bromide atoms. The resulting H-bonding networks can be described by three-dimensional supramolecular frameworks, thus forming channels in which the diprotonated amine plays a templating role. The structure can be also described as an alternation of anionic and cationic layers along the $[01\bar{1}]$ direction (Fig. 2(B)). The structure cohesion and stability is further assured by two types of hydrogen bonds, N–H···Br and C–H···Br. Compound (**2**) displays monoclinic symmetry, space group $P2_1/c$ (Table 1) with an asymmetric unit consisting of two 2(-amino methyl)pyridinium cations, four chloride anions and two water molecules as shown in Fig. 2(C). The crystal packing of the title salt, projected in the ac plane (Fig. 2(D)), shows that the organic molecule is connected with chloride anions and water molecules by N–H···Cl and N–H···O hydrogen bonds *via* nitrogen atoms. The water molecules participate in two types of hydrogen bonds O–H···Cl and N–H···O as donor or acceptor, respectively, playing a subordinative role in the stabilization of the crystal structure. All these entities form three-dimensional supramolecular frameworks and assure the stability of the structure of compound (**2**). In both title crystals, the organic cations are interlayered within the inorganic framework to compensate for the negative charge of the inorganic part. The organic parts are formed by the diprotonated amines 2-aminomethyl pyridindium cations (C–N–C = 123.64°, C–C = 1.376 to 1.505 Å, N–C = 1.343 to 1.492 Å) for (**1**) and (C–N–C = (123.10–123.18°), C–C = 1.376 to 1.5089 Å, N–C = 1.3431 to 1.477 Å) for (**2**).

The most interesting feature of the crystal structure of the two new compounds is the intermolecular hydrogen-bonding interactions and the effect of the water molecule to increase the symmetry from $P\bar{1}$ to $P2_1/c$.

3.3. Molecular Hirshfeld surfaces calculations

Hirshfeld surfaces and their associated 2D fingerprint plots were used to clarify the nature of the intermolecular interactions in $C_6H_{10}N_2$,2Br as well as $C_6H_{10}N_2$,2Cl·H_2O. The Hirshfeld surfaces have been mapped over a d_{norm}, shape-index, d_e and curvedness. The d_{norm} surface reveals the contacts of hydrogen bond donors and acceptors along with other close contacts. In d_{norm} surface, the large circular depressions (deep red) are the indicators of hydrogen bonding contacts whereas other visible spots are due to H···H contacts (Fig. 3(A) and (B)). As expected, drawing 2D fingerprint plots from the surface of the analysis presented in Fig. 4(A) and (B), the 2D fingerprint plots from Hirshfeld surface analysis allows quantitative data to be obtained on percentage of element contribution interactions in the molecule. H···Br/Br···H for compound (**1**) and H···Cl/Cl···H for compound (**2**) corresponds to 56.3% and 43.8% of the total surface structure provided by the important role of hydrogen bonds in creating strong cohesion between molecules. In addition, the decomposition of fingerprint plots H···H reaction is widespread in the two compounds (**1** and **2**) and constitutes respectively 33.1% and 36.7% of the total area of Hirshfeld surface. Moreover, a significant H···C/C···H interactions are reflected in the distribution of scattered points in the fingerprint plots, which covers 9% and 6% of the total Hirshfeld surface area for the two compounds (**1**) and (**2**), respectively. In addition, O···H/H···O interaction constitutes 4.2% of the total area of Hirshfeld surface of the $C_6H_{10}N_2$,2Cl·H_2O compound.

3.4. Biological properties

3.4.1. Antioxidant activities. Antioxidants are important compounds that reduce or neutralize free radicals, thus protecting the cells from oxidative injury.[36] Therefore, considerable research has been directed towards the identification of new antioxidants to prevent radical-induced damage. Due to various types of radicals and different sites of action, several methods

Table 3 Hydrogen bonding geometry (Å, °)[a]

	D–H (Å)	H···A (Å)	D···A (Å)	D–H···A (°)
$C_6H_{10}N_2$,2Br				
N1–H1···Br2[a]	0.86	2.39	3.2397 (17)	170
N2–H2A···Br1[b]	0.89	2.50	3.2808 (17)	146
N2–H2B···Br1[c]	0.89	2.54	3.2378 (18)	135
N2–H2C···Br2	0.89	2.62	3.3393 (17)	138
$C_6H_{10}N_2$,2Cl·H_2O				
N3–H3···Cl2	0.86	2.17	3.0296 (13)	172
N4–H4···Cl3	0.86	2.17	3.0241 (13)	177
N5–H5A···Cl1[d]	0.89	2.38	3.1809 (15)	150
N5–H5A···Cl3[e]	0.89	2.96	3.3897 (15)	112
N5–H5B···Cl2[f]	0.89	2.36	3.147 (2)	148
N5–H5B···O55	0.89	2.60	3.0603 (19)	113
N5–H5C···Cl4	0.89	2.38	3.1705 (17)	148
N6–H6A···Cl4[g]	0.89	2.38	3.1913 (15)	151
N6–H6B···O56	0.89	2.38	2.9383 (18)	121
N6–H6B···Cl1	0.89	2.38	3.2826 (18)	132
N6–H6C···Cl3[h]	0.89	2.38	3.118 (2)	158
O56–H118···Cl1[i]	0.89	2.46	3.1999 (15)	173 (3)
O55–H120···Cl4[g]	0.89	2.48	3.2039 (16)	163 (3)
O56–H119···Cl1[j]	0.84 (3)	2.39 (3)	3.212 (3)	168 (2)
O55–H121···Cl4[k]	0.86 (3)	2.35 (3)	3.190 (2)	166 (3)

[a] Symmetry codes: (a) $-x+2, -y+1, -z+1$; (b) $-x+2, -y, -z+1$; (c) $x+1, y, z$; (d) $-x+1, y+1/2, -z-1/2$; (e) $x, -y+1/2, z-1/2$; (f) $-x+1, -y, -z$; (g) $-x+1, y-1/2, -z-1/2$; (h) $-x+1, -y+1, -z$; (i) $-x+2, y+1/2, -z-1/2$; (j) $x, y+1, z$; (k) $x, y-1, z$.

Table 4 Antibacterial activity of the synthesized compounds (1) and (2) using agar disc diffusion

	Micrococcus luteus	*Salmonella enterica*	*Staphylococcus aureus*	*Bacillus cereus*	*Klebsiella pneumonia*
IZD (1)	16	10	10	22	20
IZD (2)	26	18	16	30	22
IZD (bacitracin)	19	—	25	22	9
IZD (gentamicin)	14	20	18	16	14

(with their peculiarities) are available and have been used to assess the antioxidant potential of the synthesized compounds. The antioxidant properties of the synthesized compounds (**1** and **2**) were evaluated by four different methods *in vitro*: ferric ion reducing antioxidant power (FRAP), β-carotene bleaching inhibition, DPPH (1,1-diphenyl-2-picryl-hydrazyl) and $ABTS^{+}$ 2,2′-azino-bis(3-ethylbenzthiazoline-6-sulfonic acid) radical scavenging ability (Fig. 5(A), (B), (C) and (D)). According to Li *et al.*,[37] reactive oxygen species ROS can induce cell death through mechanisms such as lipid peroxidation, alteration of cellular proteins and initiation of diverse stress-signalling pathways. Hence, to prevent free radical damage in the body, it is important to administer drugs that may be rich in antioxidants. As can be seen in the previous figures, the antioxidant activity of the synthesized compounds (**1** and **2**) increased in a concentration-dependent manner. However, the synthesized compounds showed lower antioxidant activity than did BHA and α-tocopherol, as standard, at the same concentrations. Compounds exhibited moderate antioxidant activities, they possess an almost equal potential, but the potential of the synthesized compound (**1**) was observed to be a little higher than its corresponding compound (**2**) by 53.16% (β-carotene bleaching test) and 54.23% (ABTs radical scavenging activity) and 41.46% (DPPH scavenging activity). Results of ABTS radical scavenging activity are in accordance with those of DPPH assay. At present, there is no evidence to support a mechanism for the phenomenon in the case of chloride and bromide. Therefore, it is tempting to hypothesize that the slight hight antioxidant potential of compound (**2**) is might may be hinge around the balance between reduction of metal ions to more reactive reduced forms for mediating Fenton chemistry (as is the case with some other antioxidants) and by the importance of radical-scavenging activity (antioxidant). These results obtained by preliminary screening of antioxidant activity suggested that the synthesized salts might serve as interesting compounds for the development of new antioxidant agents by synthesis of some new derivatives with these structures. Overall, compounds (**1** and **2**) displayed an important antioxidant activity. Nevertheless, they showed lower antioxidant potential than standards at the same concentration.

3.4.2. Antibacterial activity. Antibacterial activity of the synthesized compounds (**1** and **2**) was assessed against five strains. The result was compared with those of the standards (bacitracin and gentamicin) and the mean diameters of inhibition zones were shown in Table 4. From Table 4, it can be seen that the highest antibacterial activity of the synthesized compounds (**1** and **2**) against the bacterium *B. cereus* with a zone of inhibition 22 mm and 30 mm, respectively. The synthesized compounds (**1** and **2**) exhibited strong antibacterial activity against *M. luteus* with a zone of inhibition 16 mm and 26 mm, respectively, and *K. pneumonia* with a zone of inhibition 20 mm and 22 mm, respectively. However moderate activities were noted by other microbial strains with a zone of inhibition ranging between 10 mm and 18 mm. Our results have been shown that the synthesized compounds (**1** and **2**) displayed varying degrees of antimicrobial activity against Gram-positive and Gram-negative bacteria *in vitro*.

4. Conclusion

In summary, the synthesis of two new semi-organic compounds has been demonstrated. The crystal structure and biological activities have been accomplished. Our results showed that highly stable crystals were successfully prepared from an aqueous solution of (2-aminomethyl)pyridine and hydrobromic or hydrochloric acid. A meaningful structural characterization reveals that the two compounds crystallize in two centrosymmetric space groups with different arrangements. A 3D hydrogen-bonded system is built up by cationic $(2\text{-picolylamine})^{2+}$ entities as donor, Cl/Br ions and H_2O molecules as acceptors. The biological activities of the prepared compounds have been investigated. They were screened for *in vitro* antioxidant and antimicrobial activities. They have shown favourable antioxidant activities against DPPH as well as their ability to discolour the β-carotene. However, one cannot draw accurate correlations between centrosymmetric and biological activities of these materials, considering the examples presented in this paper and many more cases in literature.

Conflicts of interest

There are no conflicts to declare.

Acknowledgements

Grateful thanks are expressed to Dr T. Roisnel (Université de Rennes, CNRS, ISCR (Institut des Sciences Chimiques de Rennes) – UMR 6226, F-35000 Rennes, France) and Dr A. Roodt (Department of Chemistry, University of the Orange Free State Bloemfontein 9300, South Africa) for the X-ray data collection.

References

1 R. Swinton Darious, P. Thomas Muthiah and F. Perdih, Supramolecular hydrogen-bonding patterns in a 1 : 1 co-crystal of the N(7)–H tautomeric form of N^6-benzoyladenine with 4-hydroxybenzoic acid, *Acta Crystallogr., Sect. E: Crystallogr. Commun.*, 2017, **73**(3), 383–386.

2 K. C. Hunter, L. R. Rutledge and S. D. Wetmore, The Hydrogen Bonding Properties of Cytosine: A Computational Study of Cytosine Complexed with Hydrogen Fluoride, Water, and Ammonia, *J. Phys. Chem. A*, 2005, **109**(42), 9554–9562.

3 P. C. Singh and G. Naresh Patwari, Theoretical investigation of C–H···H–B dihydrogen bonded complexes of acetylenes with borane-trimethylamine, *Chem. Phys. Lett.*, 2006, **419**(1–3), 5–9.

4 S. R. Choudhury, P. Gamez, A. Robertazzi, C.-Y. Chen, H. M. Lee and S. Mukhopadhyay, Experimental Observation of Supramolecular Carbonyl–π/π–π/π–Carbonyl and Carbonyl–π/π–π/π–Anion Assemblies Supported by Theoretical Studies, *Cryst. Growth Des.*, 2008, **8**(10), 3773–3784.

5 M. Lozynski, Liquid water: The helical perspective of structure, *Chem. Phys.*, 2015, **455**, 1–6.

6 B.-S. Zhang and Y.-Q. Zheng, Crystal structure of 4,4′-bipyridinumdibromide, $(C_{10}H_{10}N_2)Br_2$, *Z. Kristallogr. - New Cryst. Struct.*, 2003, **218**.

7 T. V. Sundar, V. Parthasarathi, K. Sarkunam, M. Nallu, B. Walfort and H. Lang, 1-[(4-Chlorobenzoyl)methyl]-4-(*N*,*N*-dimethylamino)pyridinium bromide sesquihydrate and 1-[(4-bromobenzoyl)methyl]-4-(*N*,*N*-dimethylamino) pyridinium bromide sesquihydrate, *Acta Crystallogr., Sect. C: Cryst. Struct. Commun.*, 2004, **60**(7), o464–o466.

8 T. V. Sundar, V. Parthasarathi, K. Sarkunam, M. Nallu, B. Walfort and H. Lang, 1-[(2,4-Dichlorobenzoyl)methyl]-4-(*N*,*N*-dimethylamino)pyridinium bromide, *Acta Crystallogr., Sect. E: Struct. Rep. Online*, 2004, **60**(12), o2345–o2346.

9 T. V. Sundar, V. Parthasarathi, K. Sarkunam, M. Nallu, B. Walfort and H. Lang, 1-[2-(Biphenyl-4-yl)-2-oxoethyl]-4-(*N*,*N*-dimethylamino)pyridinium bromide hemihydrate, *Acta Crystallogr., Sect. E: Struct. Rep. Online*, 2005, **61**(4), o889–o891.

10 K. B. Kim, S. M. Yu, C. Kim and Y. Kim, 5-Carbamoyl-2-methyl-1-(2-methyl-benz-yl)pyridinium bromide, *Acta Crystallogr., Sect. E: Struct. Rep. Online*, 2012, **68**(Pt 6), o1609–o1610.

11 P. Venkatesan, V. Rajakannan and S. Thamotharan, Crystal structure of 3-amino-1-propylpyridinium bromide, *Acta Crystallogr., Sect. E: Struct. Rep. Online*, 2014, **70**(12), 580–583.

12 R. Anitha, S. Athimoolam and M. Gunasekaran, A strong NH···Br vibrational behaviour studied through X-ray, vibrational spectra and quantum chemical studies in an isomorphous crystal: 2-Nitroanilinium bromide, *Spectrochim. Acta, Part A*, 2015, **138**, 753–762.

13 A. Karthikeyan, R. Swinton Darious, P. Thomas Muthiah and F. Perdih, Supramolecular hydrogen-bonding patterns in two cocrystals of the N(7)–H tautomeric form of N^6-benzoyladenine: N^6-benzoyladenine–3-hydroxypyridinium-2-carboxylate (1/1) and N^6-benzoyladenine–DL-tartaric acid (1/1), *Acta Crystallogr., Sect. C: Struct. Chem.*, 2015, **71**(11), 985–990.

14 T. V. Sundar, V. Parthasarathi, B. Sridhar, P. Venkatesan and M. Nallu, 2-Amino-1-(4-nitrobenzyl)pyridinium bromide, *Acta Crystallogr., Sect. E: Struct. Rep. Online*, 2006, **62**(1), o74–o76.

15 P. S. Pereira Silva, M. Ramos Silva, J. A. Paixão and A. Matos Beja, *N*,*N*′,*N*″-Triphenylguanidinium bromide, *Acta Crystallogr., Sect. E: Struct. Rep. Online*, 2007, **63**(5), o2524–o2526.

16 S. M. Fellows and T. J. Prior, Crystal structure of 4-carbamoylpyridinium chloride, *Acta Crystallogr., Sect. E: Crystallogr. Commun.*, 2016, **72**(4), 436–439.

17 R. G. Lacoste and A. E. Marttel, New Multidentate Ligands. I. Coordinating Tendencies of Polyamines Contaimng α-Pyridyl Groups with Divalent Metal Ions, *Inorg. Chem.*, 1964, **3**(6), 881–884.

18 T.-M. Hseu, Y.-H. Tsai and C.-W. Cheng, Spectrophotometric Studies of Nickel(II) Chelate of 2-Picolylamine, *J. Chin. Chem. Soc.*, 1975, **22**(4), 299–308.

19 S. Utsuno and K. Sone, Spectrophotometric Studies of the Metallic Chelates of 2-Picolylamine. I. The Electronic Absorption Spectra of Some Nickel, Copper(II) and Cobalt(III) Chelates, *Bull. Chem. Soc. Jpn.*, 1964, **37**(7), 1038–1043.

20 R. P. Feazell, C. E. Carson and K. K. Klausmeyer, Variability in the Structures of Luminescent [2-(Aminomethyl)pyridine] silver(I) Complexes: Effect of Ligand Ratio, Anion, Hydrogen Bonding, and π-Stacking, *Eur. J. Inorg. Chem.*, 2005, **2005**(16), 3287–3297.

21 K. W. Törnroos, M. Hostettler, D. Chernyshov, B. Vangdal and H.-B. Bürgi, Interplay of Spin Conversion and Structural Phase Transformations: Re-Entrant Phase Transitions in the 2-Propanol Solvate of Tris(2-picolylamine)iron(II) Dichloride, *Chem.–Eur. J.*, 2006, **12**(24), 6207–6215.

22 G. M. Sheldrick, Crystal structure refinement with *SHELXL*, *Acta Crystallogr., Sect. C: Struct. Chem.*, 2015, **71**(1), 3–8.

23 G. M. Sheldrick, *SHELXT* – Integrated space-group and crystal-structure determination, *Acta Crystallogr., Sect. A: Found. Adv.*, 2015, **71**(1), 3–8.

24 L. J. Farrugia, *WinGX* and *ORTEP for Windows*: an update, *J. Appl. Crystallogr.*, 2012, **45**(4), 849–854.

25 G. M. Sheldrick, A short history of *SHELX*, *Acta Crystallogr., Sect. A: Found. Crystallogr.*, 2008, **64**(1), 112–122.

26 K. Brandenburg, *Diamond Version 3.2i*, Crystal Impact GbR, Bonn, Germany, 2012.

27 J. J. McKinnon, D. Jayatilaka and M. A. Spackman, Towards quantitative analysis of intermolecular interactions with Hirshfeld surfaces, *Chem. Commun.*, 2007, 3814.

28 M. A. Spackman and D. Jayatilaka, Hirshfeld surface analysis, *CrystEngComm*, 2009, **11**(1), 19–32.

29 M. A. Spackman and P. G. Byrom, A novel definition of a molecule in a crystal, *Chem. Phys. Lett.*, 1997, **267**(3–4), 215–220.
30 R. R. Ternavisk, A. J. Camargo, F. B. C. Machado, J. A. F. F. Rocco, G. L. B. Aquino, V. H. C. Silva, *et al.*, Synthesis, characterization, and computational study of a new dimethoxy-chalcone, *J. Mol. Model.*, 2014, **20**(12), 2526.
31 B. Wang, Z.-R. Li, C.-F. Chi, Q.-H. Zhang and H.-Y. Luo, Preparation and evaluation of antioxidant peptides from ethanol-soluble proteins hydrolysate of Sphyrna lewini muscle, *Peptides*, 2012, **36**(2), 240–250.
32 I. I. Koleva, T. A. van Beek, J. P. H. Linssen, A. de Groot and L. N. Evstatieva, Screening of plant extracts for antioxidant activity: a comparative study on three testing methods, *Phytochem. Anal.*, 2002, **13**(1), 8–17.
33 Z. Xie, J. Huang, X. Xu and Z. Jin, Antioxidant activity of peptides isolated from alfalfa leaf protein hydrolysate, *Food Chem.*, 2008, **111**(2), 370–376.
34 P. Bersuder, M. Hole and G. Smith, Antioxidants from a heated histidine-glucose model system. I: Investigation of the antioxidant role of histidine and isolation of antioxidants by high-performance liquid chromatography, *J. Am. Oil Chem. Soc.*, 1998, **75**(2), 181–187.
35 J. R. Tagg and A. R. McGiven, Assay System for Bacteriocins, *Appl. Microbiol.*, 1971, **21**(5), 943.
36 S. Farooq and F. Azam, The use of cell membrane stability (CMS) technique to screen for salt tolerant wheat varieties, *J. Plant Physiol.*, 2006, **163**(6), 629–637.
37 S. Li, X. Li and G. J. Rozanski, Regulation of glutathione in cardiac myocytes, *J. Mol. Cell. Cardiol.*, 2003, **35**(9), 1145–1152.